High-frequency Subband Compressed Sensing MRI

K. Sung[1], and B. A. Hargreaves[1]
[1]Radiology, Stanford University, Stanford, California, United States

Introduction: Compressed sensing (CS) is an acquisition and reconstruction technique that can dramatically reduce the measurement size [1]. Its promise to improve imaging speed of MRI has been successfully demonstrated with the wavelet transform [2]. However, conventional CS MRI still suffers from: possible reconstruction failure causing residual incoherent artifacts, image quality degradation resulting in poorer spatial resolution, and complicated integration with other existing acceleration methods. Wavelet subbands typically contain different sparsities due to multi-resolution analysis and wavelet-tree structure; high-frequency subbands (Fig 1: HL, LH, and HH) are the largest and most sparse regions in the wavelet. Separate *Fourier* sampling of each wavelet subband exploits this subbands sparsity in acquisition and can improve reconstruction performance [3]. Here, we present a new method, which applies CS to only high-frequency subbands to maximally utilize the wavelet characteristics while minimizing reconstruction artifacts, and allowing easy incorporation of other rapid imaging techniques.

Theory: Let Φ denote the undersampled *Fourier* measurement matrix, Ψ the wavelet transform (J is the finest scale), and w_n the wavelet coefficients on subband n. The acquired data y can be decomposed into k-space data generated from each wavelet subband:

$$\mathbf{y = y_{J,HL} + y_{J,LH} + y_{J,HH} + y_{J-1,HL} + y_{J-1,LH} + y_{J-1,HH} + y_{LL}}$$

where y_n is k-space data generated from wavelet coefficients on subband n, and y_{LL} is a sum of y_n, n = 0,..,J-2. y_n after reweighting (by the *Fourier*-wavelet spectrum) is simply the undersampled *Fourier* transform of w_n, and therefore separate CS can be performed for each w_n.

Methods: Identical incomplete k-space data should be acquired on each wavelet subband (for scale J-1 and J) to be able to decompose y_n from y.

I. Sampling Mask Generation (Fig 2):

1. Generate a random sampling mask (m_{J-1}: n/4 × n/4) by a reduction factor of 8 – 10.
2. Tile m_{J-1} on a 3 × 3 grid and crop it so that the final size is twice the original (m_J: n/2 × n/2).
3. Tile m_J on a 3 × 3 grid and crop it (m: n × n) with adding full sample region (n/2 × n/2). m is the final k-space sampling with the overall reduction factor (R) of 2.9 – 3.2.

II. High-frequency Subband CS:

1. Estimate k-space content (y_{LL}). Since the fully sampled region (white box) covers almost all-spectral weighting, estimation y_{LL} using a zero filling reconstruction is nearly perfect. Compute the residual by subtracting y_{LL} from y ($\Delta y = y - y_{LL}$).
2. Decompose y_n from Δy using m_{J-1}.
3. Apply CS for y_n after reweighting to estimate w_n. L_1 minimization is performed three separate times (for HL, LH, and HH) using m_J.
4. Compute k-space content ($y_{J,HL}$, $y_{J,LH}$, and $y_{J,HH}$), and subtract them from Δy. Use inverse *Fourier* and wavelet transforms to calculate wavelet coefficients on J-1 scale.

Daubechies-8 wavelets were used as a sparsifying transform with 3 wavelet scales (J=3). Constrained L_1 minimization was solved by L_1-regularized least squares method [4]. Fully sampled phantom and brain data (512 × 512) with sampling mask (both frequency directions were randomly selected) were used to validate the method (R = 2.9).

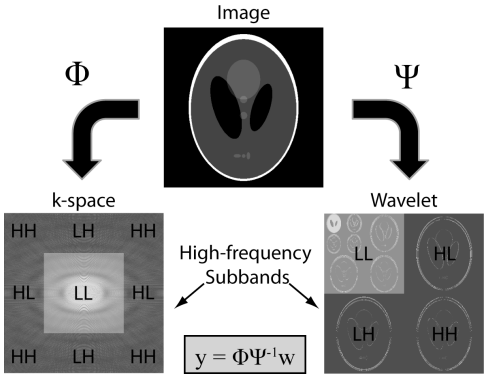

Figure 1: The relationship between *Fourier* (Φ) and wavelet (Ψ) transforms. High-frequency subbands (HL, LH, HH) are both shown in the Fourier and wavelet domains.

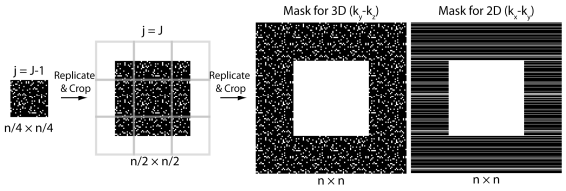

Figure 2: Generation of k-space sampling patterns (m: n × n) for HiSub CS.

Results and Discussion: Fig 3 shows reconstruction results for phantom and human brain data. In phantom images, the high-frequency subband (HL) shows that non-zero coefficients were recovered by using HiSub CS, and high-frequency components in k-space were well synthesized. The difference in the reconstructed images is subtle due to the fully acquired low-frequency region, but HiSub CS carries high-resolution structures whereas the zero-filling image does not. The regular CS similarly synthesizes high-frequency content but was less accurate than HiSub CS (images not shown). In a brain example, HiSub CS maintains fine structures and the reconstructed image is almost identical to original. Note that L_1 minimization naturally denoises outcomes, and different k-space regions have different denoising effects (low-frequency: no denoising and high-frequency: denoising). Extension to parallel imaging is simple because random and fully sampled areas are clearly separated. The method is also robust to reconstruction error since CS only involves in high-frequency region and possible errors on high-frequency components have minimal effects on anatomical structures (i.e. no worse than zero filling).

Conclusion: The proposed method considers variation in wavelet-domain sparsity and applies separate acquisition and reconstruction for high- and low-frequency subbands. The reconstructed images recover fine structures with successful reconstruction of each wavelet subband while image artifacts are restricted to high spatial frequencies.

Acknowledgments: GE Healthcare and NIH P41 RR 009784

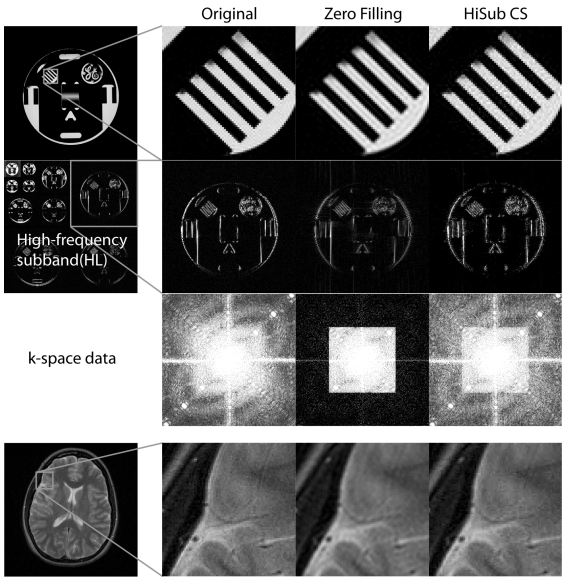

Figure 3: Examples of HiSub CS reconstruction for phantom and brain data (R=2.9).

Reference: [1] Donoho, IEEE TIT, 2006;52(4):1289, [2] Lustig et al., MRM, 2007;58:1182, [3] Candes et al., Inverse Problems, 2007;23:969, [4] Kim et al., IEEE JSTSP, 2007;1(4):606